Revista Colombiana de Química
ISSN: 0120-2804
ISSN: 2357-3791
rcolquim_fcbog@unal.edu.co
Universidad Nacional de Colombia
Colombia

Electrochemical analysis of the corrosion inhibition properties of L-leucine and trypsin complex admixture on high carbon steel in 1 M H_2SO_4 solution

Loto, Roland T.

Electrochemical analysis of the corrosion inhibition properties of L-leucine and trypsin complex admixture on high carbon steel in 1 M H_2SO_4 solution

Revista Colombiana de Química, vol. 47, no. 2, 2018

Universidad Nacional de Colombia, Colombia

Available in: https://www.redalyc.org/articulo.oa?id=309055565002

DOI: https://doi.org/10.15446/rev.colomb.quim.v47n2.68058

Aplicada y Analítica

Electrochemical analysis of the corrosion inhibition properties of L-leucine and trypsin complex admixture on high carbon steel in 1 M H_2SO_4 solution

Análisis electroquímico de las propiedades de inhibición de la corrosión de la mezcla de L-leucina y complejo de tripsina sobre acero de alto contenido de carbono en solución 1 M de H_2SO_4

Análise eletroquímica das propriedades de inibição da corrosão da mistura de L-leucina e complexo de tripsina em aço de alto carbono em solução 1 M de H_2SO_4

Roland T. Loto
Covenant University, Nigeria
tolu.loto@gmail.com

DOI: https://doi.org/10.15446/rev.colomb.quim.v47n2.68058
Redalyc: https://www.redalyc.org/articulo.oa?id=309055565002
Received: 28 September 2017
Accepted: 17 November 2017

Abstract:

Corrosion inhibition of biodegradable chemical compounds (L-leucine and trypsin complex) on high carbon steel in 1 M H_2SO_4 acid media was evaluated with potentiodynamic polarization technique, weight loss analysis, open circuit potential measurement, optical microscopy, and ATR-FTIR spectroscopy. Data obtained showed the mixture has a maximum inhibition efficiency of 82.4% and 90.08% from the electrochemical tests with mixed type inhibition properties. The addition of the mixture shifts significantly the corrosion potential of the steel to passivation values from open circuit potential measurement. Results from thermodynamic calculations indicated chemisorption adsorption mechanism according to Langmuir, Freundlich, and Frumkin isotherms coupled with correlation coefficients of 0.9994, 0.9651 and 0.8834. Statistical analysis showed exposure time to be the most significant variable responsible for corrosion inhibition. Identified functional groups of the compound from ATF-FTIR spectroscopy were adsorbed completely on the carbon steel surface from observation of the decreased peak intensity. Optical microscopy images of the inhibited and uninhibited steel surfaces contrast each other with due to the presence of macro-pits and porous oxide on the uninhibited steel.

Keywords: corrosion, carbon steel, sulphuric acid, L-leucine, trypsin complex.

Resumen:

Se evaluó la inhibición de la corrosión por parte de compuestos químicos biodegradables (complejo de L-leucina y tripsina) sobre acero de alto contenido de carbono en H_2SO_4 1 M a través de técnica de polarización potenciodinámica, análisis de pérdida de peso, medición de potencial de circuito abierto, microscopía óptica y espectroscopia ATR-FTIR. Los datos obtenidos mostraron que la mezcla tiene una eficacia de inhibición máxima de 82,4% y 90,08%, a partir de las pruebas electroquímicas con propiedades de inhibición de tipo mixto. La adición de la mezcla cambia significativamente el potencial de corrosión del acero a los valores de pasivación de la medición del potencial de circuito abierto. Los resultados de los cálculos termodinámicos indicaron un mecanismo de adsorción por quimisorción de acuerdo con las isotermas Langmuir, Freundlich y Frumkin, acopladas con coeficientes de correlación de 0,9994; 0,9651 y 0,8834, respectivamente. El análisis estadístico mostró que el tiempo de exposición es la variable más importante en la inhibición de la corrosión. Los grupos funcionales de la mezcla, identificados mediante espectroscopía ATF-FTIR, fueron completamente adsorbidos en la superficie de acero al carbono; esto se dedujo a partir de la observación de la disminución de la intensidad de pico. Las imágenes de microscopía óptica de las superficies de acero inhibidas y desinhibidas contrastan entre sí, debido a la presencia de macro-pozos y óxido poroso en el acero desinhibido.

Palabras clave: corrosión, acero carbono, ácido sulfúrico, L-leucina, complejo de tripsina.

Resumo:

Author notes

tolu.loto@gmail.com

Foram feitos estudos de inibição da corrosão de compostos químicos biodegradáveis ccomplexo de L-leucina e tripsina) em aço de alto conteúdo de carbono em meio de H_2SO_4 1 M, estes foram avaliados com técnica de polarização potenciodinâmica, análise de perda de peso, medição de potencial de circuito aberto, microscopia óptica e espectroscopia ATR-FTIR. Os dados obtidos mostram que a mistura tem uma eficiência de inibição máxima de 82,4% e 90,08% dos testes eletroquímicos com propriedades de inibição do tipo misto. A adição da mistura desloca significativamente o potencial de corrosão do aço para valores de passivação da medição de potencial de circuito aberto. Os resultados dos cálculos termodinâmicos indicam o mecanismo de adsorção de quimisorção de acordo com as isotermas de Langmuir, Freundlich e Frumkin, juntamente com coeficientes de correlação de 0,9994; 0,9651 e 0,8834 respectivamente. A análise estatística mostrou que o tempo de exposição é a variável mais significativa da inibição da corrosão. Os grupos funcionais identificados pela espectroscopia ATF-FTIR foram completamente adsorvidos na superfície do aço ao carbono, de acordo com a observação da intensidade de pico diminuída. As imagens de microscopia óptica das superfícies de aço inibidas e desinibidas contrastam entre si devido à presença de macro-poços e óxido poroso no aço desinibido.

Palavras-chave: corrosão, Aço carbono, ácido sulfúrico, L-leucina, complexo de tripsina.

Introduction

High carbon steel is one of the most common steel types due to its relatively low cost and high strength, while it provides material properties acceptable in many applications. However, its sustainable use is limited by its low corrosion resistance in industrial environments such as acid cleaning, pickling, descaling, and drilling operations in oil and gas exploration (*1* , *2* , *3*). One of the fundamental causes of corrosion is the reduction in the value of Gibbs free energy of the materials.

Production of almost all engineering material components made of metals involves the addition of energy to the metals in the unrefined form. The metals tend to be highly reactive due to the fewer number of valence electrons, thus they lose their electrons during chemical and electrochemical reactions. The corrosion damage results basically from the interaction of metallic structures with their environment (*4*).

In some cases, corrosion damage is tolerable and leads to higher maintenance costs with minimal losses. However, corrosion can also result in catastrophic failures with loss of life and downtime of industrial services. Deterioration of metallic surfaces reduces the efficiency of metallic equipment resulting in financial loss to industries. To alleviate the damaging effects of corrosive anions and other constituents in industrial environments, the use of corrosion inhibitors has been proven to be a comparatively cost-effective solution (*5* , *6*). Organic compounds with N, O, and S atoms are considered to be effective corrosion inhibitors; their effectiveness depends on the chemical composition and structure of the compound. However, the toxic nature and relatively high cost of organic inhibitors emphasize the need for sustainable alternatives. Application of low-cost and eco-friendly compounds as corrosion inhibitors have gradually replaced their toxic counterparts in recent years (*7* , *8, 9, 10, 11, 12* , *13, 14*). In such way, this research aims to study the corrosion inhibiting properties and performance of the combined admixture of L-leucine and trypsin complex on high carbon steel in dilute sulphuric acid.

Materials and Methods

AISI 1095 High carbon steel (1095HCS) obtained commercially with nominal (wt.%) composition shown in Table 1 has a cylindrical shape with average dimensions of 0.71 cm length, 1.4 cm diameter and 5.94 cm^2 surface area. The carbon steel samples were machined first to the final shape and then grinded with silicon carbide abrasive papers of 80, 320, 600, 800 and 1000 grit. They were subsequently washed with distilled water and acetone. The samples then were stored in a desiccator for weight loss analysis, potentiodynamic polarization technique, and corrosion potential measurement according to ASTM G1-03 (*15*).

L-leucine (figure 1) obtained from Sigma Aldrich USA is a white powdery solid with a molar mass of 131.17 g/mol and a molecular formula of $C_6H_{13}NO_2$. Trypsin complex obtained from Bell, Sons & Co. Ltd

UK is a transparent oily liquid with a molar mass of 933.45 g/mol and a molecular formula of $C_{57}H_{104}O_9$. The molecular structure of both compounds is shown in Figure 1a and b. Their combined admixture (LTC) was prepared in volumetric concentrations of 1%, 2%, 3%, 4% and 5% LTC per 200 mL of 1 M H_2SO_4 acid prepared from analytical grade (98%) with distilled water.

Table 1. Percentage Nominal Composition of AISI 1095 carbon steel.

Element Symbol	Mn	P	S	C	Fe

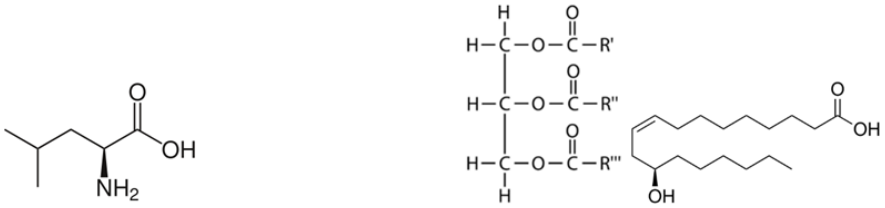

(a) (b)

Figure 1. Molecular structure of (a) L-leucine and (b) Trypsin complex (triester of glycerol and ricinoleic acid).

Potentiodynamic polarization curves were obtained at a scan rate of 0.0015 V/s between potentials of −1.5 V and +1.5 V and then plotted according to ASTM G102-89 (16). A platinum rod was used as the counter electrode and a silver chloride electrode (Ag/AgCl) as the reference electrode. Corrosion current density (J_{cr}, A/cm^2) and corrosion potential (E_{cr}, V) values were obtained from Tafel extrapolation of the polarization curves. The corrosion rate (C_R) and the inhibition efficiency (h) were calculated from the formula below (Eq. [1]):

$$C_R = \left[\frac{87.6\omega}{DAt}\right] \qquad [2]$$

Where D is the density in g/cm^3; Eqv is the sample equivalent weight in grams. 0.00327 is a constant for corrosion rate calculation in mm/year (*17*). 1095HCS samples immersed individually in 200 mL of the 1 M H_2SO_4/1% - 5% LTC solutions for 360 h at 30 oC ambient temperature were weighed at 24 h interval according to ASTM G31-72 (*18*). Corrosion rate (C_R) was determined from the mathematical relationship below (Eq. [2]) (*19*):

$$C_R = \frac{0.00327 \times J_{cr} \times E_{qv}}{D} \qquad [1]$$

Where ω is the weight loss in mg, D is the density in g/cm^3, A is the total surface area of the coupon in cm^2 and 87.6 is a constant for corrosion rate determination in mm/year; and t is the time in h. Inhibition efficiency (h) was determined from the equation below (Eq. [3]):

$$C_R = \left[\frac{87.6\omega}{DAt}\right] \qquad [2]$$

Where ω_1 and ω_2 are the weight loss at specific LTC concentrations. Surface coverage was determined from the formula below (Eq. [4]) (*20* , *21*):

$$\eta = \left[\frac{\omega_1 - \omega_2}{\omega_1}\right] \times 100 \qquad [3]$$

Where ϑ is the degree of LTC mixture, adsorbed per gram of 1095HCS surface; ω_1 and ω_2 are the weight loss of each 1095HCS sample at specific concentrations of LTC in the acid solution.

1 M H_2SO_4/LTC solutions (before and after 1095HCS corrosion) were exposed to a specific range of infrared ray beams from Bruker ALPHA FTIR spectrometer at the wavelength range of 375 to 7500 cm^{-1} and resolution of 0.9 cm^{-1}. The transmittance and reflectance of the infrared beams at various frequencies were decoded and transformed into an ATF-FTIR absorption plot consisting of spectra peaks. The spectral pattern was evaluated and equated with ATF-FTIR absorption table to identify the LTC functional groups actively involved in corrosion inhibition. Micro-analytical images (surface morphology and topography) of LTC inhibited and corroded 1095HCS samples were studied with an Omax 40X-2500X Plan Infinity Trinocular Metallurgical microscope through the aid of ToupCam analytical software.

Statistical studies through analysis of variance (ANOVA) at a confidence level of 95% (significance level of $\alpha = 0.05$) was employed to assess the statistical significance of LTC concentration and exposure time on the calculated corrosion rate values of HCS in 1 M H_2SO_4 solutions according to the mathematical relationships (Eqs. [2] [3] [4] [5] [6]).

The Sum of squares among columns (Exposure time):

$$\theta = \left[1 - \frac{\omega_2}{\omega_1}\right] \qquad [4]$$

Sum of Squares among rows (LTC concentration):

$$SS_c = \frac{\sum T_c{}^2}{nr} - \frac{T^2}{N} \qquad [5]$$

Total Sum of Squares:

$$SS_r = \frac{\sum T_r{}^2}{nc} - \frac{T^2}{N} \qquad [6]$$

Results and Discussion

Polarization studies

Corrosion polarization plots of the anodic-cathodic behavior of HCS in 1 M H_2SO_4/1% - 5% LTC are shown in Figure 2. Potentiodynamic polarization data obtained are presented in Table 2. The corrosion current density at 0% LTC (1.59 x 10^{-3}Acm^{-2}) was drastically reduced to 3.88 x 10^{-4} Acm^{-2} at 1% LTC due to the electrochemical action of ionized LTC molecules in retarding the electrolytic transport of SO_4^{2-} ions unto the steel surface.

Further increase in LTC concentration (2% - 5% LTC) caused a proportionate decrease in corrosion current density to 2.79 x 10^{-4} at 5% LTC. This corresponds to a corrosion rate value of 3.24 mm/year in comparison to 18.42 mm/year at 0% LTC. The corrosion potential values (Table 2) showed the mixed inhibition properties of LTC. At 0% LTC, the polarization plots shifted cathodically from -0.298 V to -0.224 V (1% LTC) before shifting in the anodic direction (2% - 5% LTC) due to the dominant anodic inhibiting action of LTC mixture, through surface coverage and adsorption, resulting from charge transfer, whereby the hydrogen evolution and oxygen reduction reactions are stifled (*22*).

The analysis of the Tafel slopes suggests a significant difference between the values of the steel exposed to 0% LTC and 1% LTC confirming the strong influence of LTC on the redox electrochemical process occurring on HCS surface. Further increase in LTC concentration did not affect significantly either the values of the Tafel slopes. The anodic Tafel slopes are much greater than the respective cathodic Tafel slopes due to its higher anodic exchange-current density values compared to the cathodic values.

LTC proved to be an effective inhibiting compound at the concentrations studied with inhibition efficiency ranging from 75.59% to 82.40%. A lone pair of electrons is available on the oxygen atoms, and hence, a coordination of the ionized inhibitor molecules with HCS metal atoms. Electrons flow from the electron rich centers of LTC to electron deficient centers of HCS metal inhibiting the electrochemical processes responsible for corrosion. As concentration increases in LTC, increased marginally its inhibition efficiency showing it is slightly concentration dependent. The maximum change in corrosion potential of HCS in the anodic and cathodic direction is less than 85 mV, thus LTC is a mixed type inhibitor (*23* , *24*).

Table 2. Potentiodynamic polarization result for HCS in 1 M H2SO4/0% - 5% LTC.

Sample	LTC Conc. (%)	LTC Conc. (M)	Corrosion Rate (mm/year)	LTC Inhibition Efficiency (%)	Corrosion Current (A)	Corrosion Current Density (A/cm^2)	Corrosion Potential (V)	Polarization Resistance, R_p (Ω)	Cathodic Tafel Slope, B_c (V/dec)	a
A	0	0	18.42	0	2.45E-03	1.59E-03	-0.298	71.47	-9.682	0.704
B	1	9.39 E-03	4.50	75.59	5.97E-04	3.88E-04	-0.224	740.35	-7.317	1.520
C	2	1.88 E-02	4.13	77.56	5.49E-04	3.56E-04	-0.319	560.15	-6.463	1.106
D	3	2.82 E-02	3.82	79.28	5.07E-04	3.29E-04	-0.303	676.15	-6.781	1.220
E	4	3.76 E-02	3.46	81.20	4.60E-04	2.98E-04	-0.290	885.13	-6.545	1.391
F	5	4.70 E-02	3.24	82.40	4.30E-04	2.79E-04	-0.283	1332.13	-6.604	1.808

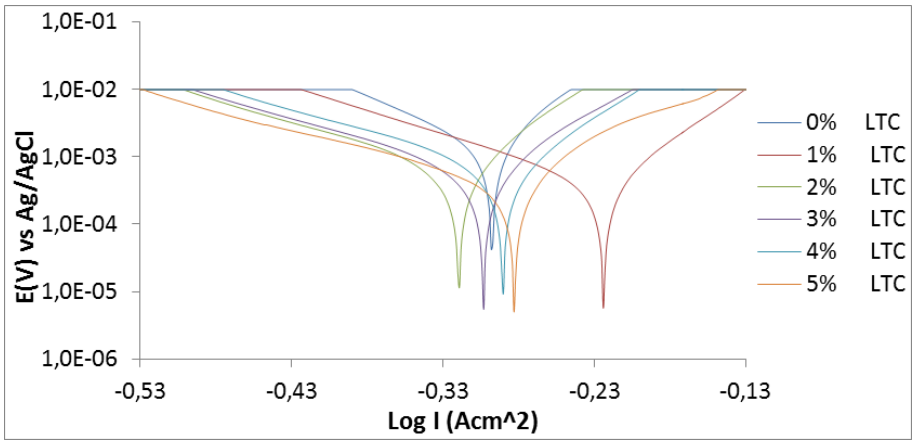

Figure 2. Potentiodynamic polarization plots for HCS in 1 M H_2SO_4/0% - 5% LTC.

Open circuit potential measurement

Plots of graphs of corrosion potential versus exposure time for HCS specimens in 1 M H_2SO_4/ 0% LTC, 1 M H_2SO_4/ 1% LTC, and 1 M H_2SO_4/ 5% LTC for 1800 s are shown in Figure 3. The corrosion potential values for HCS in 1 M H_2SO_4/ 0% LTC started at -0.363 $V_{Ag/AgCl}$ at 0 s and changed progressively till -0.334 $V_{Ag/AgCl}$ at 1800 s due to active polarization reactions on the steel surface. Addition of LTC to the acid solution changed the dynamics of the redox electrochemical reactions in the debilitating actions presence of SO_4^{2-} anions. HCS in 1 M H_2SO_4/ 1% and 5% LTC solution showed similar open circuit corrosion potential behavior between 0 s and 1800 s, but contrast significantly the corrosion behavior of HCS in 1 M H_2SO_4/ 0%. At 0 s their corrosion potential values were -0.276 $V_{Ag/AgCl}$ and -0.239 $V_{Ag/AgCl}$; the values decreased progressively to -0.301 $V_{Ag/AgCl}$ and -0.319 $V_{Ag/AgCl}$ at 1250 s. Beyond 1250 s the corrosion potential values varied marginally. The difference in corrosion potential despite similar active/passive corrosion behavior between 1% and 5% LTC is the result of differences in LTC concentration. Increase in LTC concentration shifted the graphical plot of HCS reaction in H_2SO_4 solution due to adsorption of LTC molecules which inhibits further corrosion reaction on HCS surface.

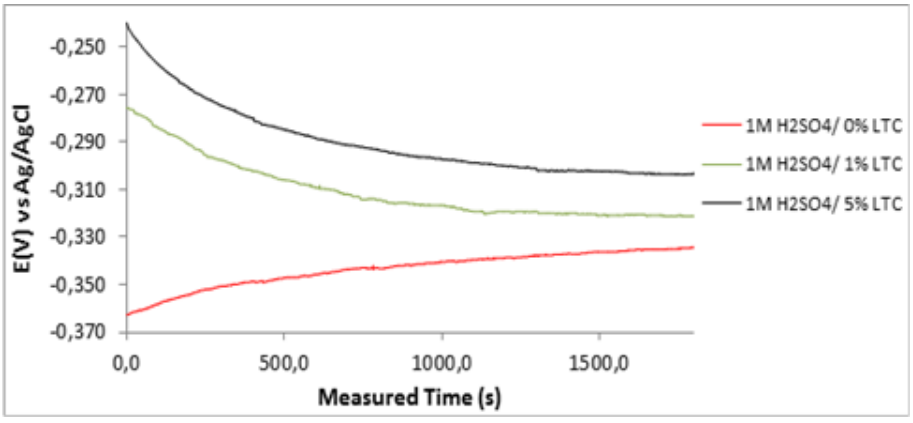

Figure 3. Variation of corrosion potential versus measured time for HCS specimen immersed in 1 M H2SO4/0%, 1% and 5% LTC.

Adsorption isotherm studies

Corrosion inhibition of HCS in dilute 1 M H_2SO_4/LTC solution occurs when LTC molecules accumulate on HCS surface forming a molecular or atomic film; LTC inhibition efficiency is due to the strength of its adsorption. The electrochemical action of LTC molecules on HCS surfaces with respect to concentration can be further understood through adsorption isotherms. The isotherms relate the amount of LTC mixture from aqueous acid solution with its concentration at the metal/solution interphase at constant temperature and pH (*25* , *26*). Langmuir, Frumkin, and Freundlich isotherms gave the best fitting for LTC adsorption on HCS surface from correlation the coefficient values obtained.

Langmuir isotherm model suggests the presence of a fixed number of vacant or adsorption sites on the metallic surface, of equal dimension and shape on the metal surface holding a specific amount of inhibitor molecule. This results in the release of definite amount of heat energy. The isotherm also suggests the non-existence of lateral interaction between the adsorbed molecules (*27*). Figure 4 shows the plots of $\frac{C_{LTC}}{\theta}$ vs CLTC agrees with the Langmuir isotherm, with a correlation coefficient of 0.9994 according to the Langmuir equation [8].

$$\theta = \left[\frac{K_{LTC}C_{LTC}}{1+K_{LTC}C_{LTC}}\right] \qquad [8]$$

Where ϑ is the amount of LTC adsorbed per unit gram on HCS surface at equilibrium surface coverage. C_{LTC} is LTC inhibitor concentration, and K_{LTC} is the equilibrium constant of adsorption.

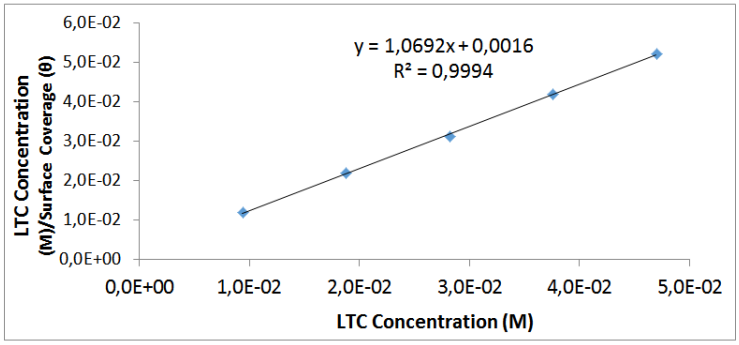

Figure 4. Langmuir isotherm plot of $\frac{C_{LTC}}{\theta}$ versus LTC concentration in 1 M H_2SO_4.

The Frumkin isotherm model assumes metallic surfaces to be non-homogeneous and the lateral interaction effect among adsorbed LTC molecules is apparent according to the equation [9] (*28*):

$$\theta/_{1-\theta} = K_{LTC}C_{LTC}e^{2\alpha\theta} \qquad [9]$$

Rearranging [9] the equation becomes [10]:

$$\log\left[\theta/_{(1-\theta)C_{LTC}}\right] = 2.303 \log K_{LTC} + 2\alpha\theta \qquad [10]$$

Where α is the interaction parameter which describes the molecular interaction in the adsorbed layer, and calculated from the slope of the Frumkin isotherm plot. For positive α adsorption energy increases with ϑ, whereas for negative α adsorption energy decreases with ϑ. K_{LTC} is the adsorption-desorption constant. In Figure 5 plots of log $[\theta/(1-\theta)c_{LTC}]$ versus ϑ showed a correlation coefficient of 0.9651 in 1 M H_2SO_4 solution.

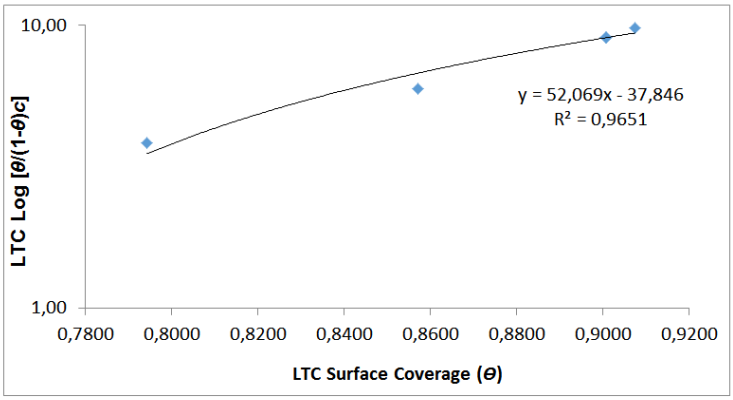

Figure 5. Frumkin isotherm plot of $\log\left[\theta/(1-\theta)c_{LTC}\right]$ versus surface coverage (θ) in 1 M H_2SO_4.

Freundlich isotherm defines the relationship between adsorbed LTC molecules, their interaction and influence on the adsorption process through molecular repulsion or attraction according to the following equations ([11] and [12]):

$$\theta = K_{LTC} C_{LTC}^{n} \qquad [11]$$

$$\log \theta = n \log C_{LTC} + \log K_{LTC} \qquad [12]$$

Where n is a constant depending on the characteristics of the adsorbed molecule and K_{LTC} is the adsorption-desorption equilibrium constant denoting the strength of interaction in the adsorbed layer. The amount adsorbed on HCS surface represents the sum total of adsorption on the reactive sites (*29* , *30*). The correlation coefficient for Freundlich isotherm plot (Figure 6) is 0.8834.

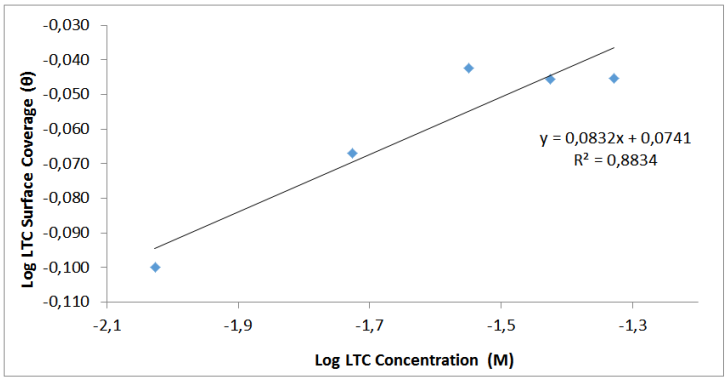

Figure 6. Freundlich isotherm plot of log LTC surface coverage versus Log LTC concentration in 1 M H_2SO_4.

.

Thermodynamics of the corrosion inhibition mechanism

The intermolecular reaction of LTC on HCS surface and the adsorption type was determined from the thermodynamics of LTC reaction with HTC surface through the Langmuir isotherm due to its correlation coefficient being closest to unity. Calculated results of Gibbs free energy of adsorption in H_2SO_4 solution is shown in Table 3, from Equation [13] (*31*):

$$\Delta G_{ads} = -2.303RT \log [55.5K_{LTC}] \qquad [13]$$

Where 55.5 is the molar concentration of water in the acid solution, R is the universal gas constant, T is the absolute temperature, and K_{LTC} is the equilibrium constant of LTC adsorption on HCS. Negative values of ΔG°_{ads} depict the spontaneity and stability of the adsorption mechanism. The lowest ΔG°_{ads} value is -40.11 KJmol^{-1} at the highest LTC concentration, while the highest ΔG°_{ads} value is -41.99 KJmol^{-1} at the lowest LTC concentration on HCS surface due to the effect of lateral repulsion among LTC molecules at higher LTC concentration. The ΔG°_{ads} values calculated shows chemisorption adsorption mechanisms on HCS surface (*32* , *33*).

Table 3. Results for Gibbs free energy (ΔG°_{ads}), surface coverage (θ) and equilibrium constant of adsorption (K_{ads}) for LTC adsorption on HCS in 1 M H_2SO_4 solution.

Samples	LTC Concentration (M)	Surface Coverage (θ)	Equilibrium Constant of adsorption (K_{LTC})	-1
A	0	0	0	0
B	9.39E-03	0.794	411373.8	-41.99
C	1.88E-02	0.857	319471.7	-41.36
D	2.82E-02	0.907	347919.9	-41.57
E	3.76E-02	0.901	241192.7	-40.66
F	4.70E-02	0.901	193285.3	-40.11

ATF-FTIR Spectroscopy analysis

Functional groups within LTC mixture involved in the corrosion inhibition and adsorption reactions on HCS were identified by ATF-FTIR spectroscopy after being equated with the ATR-FTIR Theoretical Tabla (*34* , *35*). Figure 7 shows the spectra plots of 1 M H_2SO_4/LTC solution before and after HCS corrosion. The transmittance of calculated wavenumbers of 1 M H_2SO_4/LTC solution before corrosion at intervals of 2981.97 – 3518.41 cm^{-1}, 1066.74 – 1150.37 cm^{-1}, and 542.55 – 724.08 cm^{-1} decreased significantly after corrosion due to corrosion inhibition resulting from adsorption of specific LTC functional groups. Identified functional groups of alcohols, phenols, primary and secondary amines and amides, carboxylic acids, alkynes, aromatics, alkenes, and alkanes consisting of bonds such as O–H stretch, free hydroxyl, H–bonded, N–H stretch, –C(triple bond)C–H: C–H stretch, C–H stretch and =C–H stretch bonds where responsible for the corrosion inhibition of HCS steel. The increased transmittance of the functional groups at other wavenumbers shows that surface coverage was also significantly responsible for corrosion inhibition of HCS.

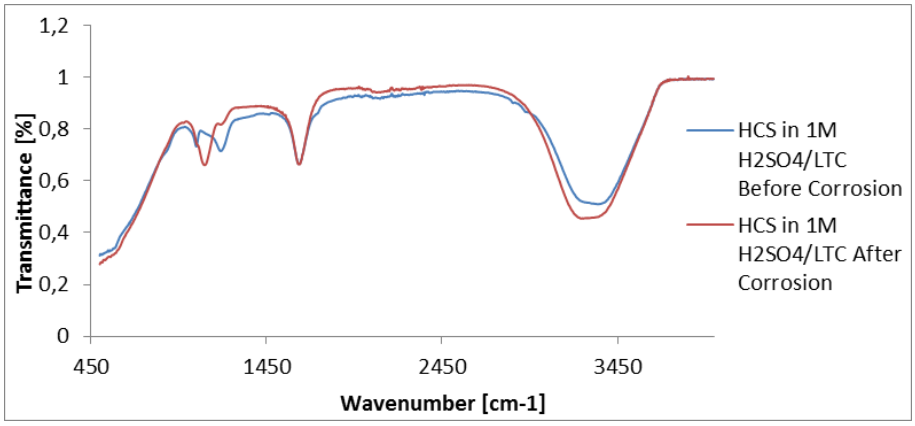

Figure 7. ATF-FTIR spectra of 1 M H_2SO_4/ LTC solution before and after HCS corrosion.

Weight loss measurement and micro-analytical studies

Experimental data for weight loss (ω), corrosion rate (C_R) of HCS, and LTC inhibition efficiency (#) in 1 M H_2SO_4 solution at 360 h exposure time are shown in Table 4. Figure 8 (a and b) depicts the plot of HCS corrosion rate and LCN inhibition efficiency versus exposure time (24 h – 360 h). Micro-analytical images of HCS before and after corrosion, in the presence and absence of LTC, are shown in Figures 9 (a) to 10 (b) at mag. x100. The corrosion rate values of HCS at 0% LTC was unstable [Figure. 8(a)] for the first 120 h, alternating from 0.0121 mm/year at 24 h to 0.0128 mm/year. A consistent decrease in corrosion rate was later observed after 120 h, till 216 h decreased for the first 72 h of exposure to 0.0081 mm/year before increasing progressively to 0.011 mm/year at 288 h due to the redox electrochemical action of SO_4^{2-} ions resulting from the disassociation of H_2SO_4 in H_2O (Eqs. [14a] and [14b]). Further exposure of HCS in the acid solution beyond 216 h caused a progressive increase in corrosion rate values till 360 h (0.0136 mm/year), during which severe anodic dissolution and deterioration of HCS surface morphology (Figure 9(d)) occurred according to Eq. [15]. The presence of porous oxides and corrosion pits are clearly visible on HCS surface.

$$H_2SO_{4(aq)} + H_2O_{(l)} \rightarrow H_3O^+_{(aq)} + HSO_4^-{}_{(aq)} \qquad [14a]$$

The HSO_4^- ion also dissociates to a small degree:

$$HSO_4^- + H_2O \rightarrow H_3O + SO_4^{2-} \qquad [14b]$$

$$Fe_{(s)} + 2H_2SO_{4(aq)} \rightarrow FeSO_{4(aq)} + H_{2(g)} \qquad [15]$$

The optical microscopic images in Figure 10 (a and b) show a slightly degraded surface at 1% and 5% LTC as compared to the surface morphology in Figure 9 (b). This observation is due to the inhibiting action of LTC mixture at the concentrations studied. The slight deterioration earlier mentioned is probably due to the initial preadsorbed SO_4^{2-} ions on HCS surface before the electrolytic transport and adsorption of LTC on the steel surface, which stifled further redox electrochemical reactions. The inhibition performance of LTC

appears to be time-dependent rather than concentration dependent [Figure 8 (b)]. The inhibition efficiency values tend to increase with time, attaining peak inhibition efficiency (360 h) of 79.44 mm/year and 90.08 mm/year at 1% and 5% LTC.

Table 4. Experimental data from weight loss measurement at 360 h for HCS corrosion in 1 M H_2SO_4 media (0% - 5% LTC).

Samples	Weight Loss (g)	LTC Conc. (%)	LTC Conc. (M)	Corrosion Rate (mm/year)	LTC Inhibition Efficiency (%)
A	2.608	0	0	0.0136	0
B	0.536	1	9.39E-03	0.0028	79.44
C	0.373	2	1.88E-02	0.0019	85.72
D	0.241	3	2.82E-02	0.0013	90.74
E	0.259	4	3.76E-02	0.0014	90.06
F	0.259	5	4.70E-02	0.0014	90.08

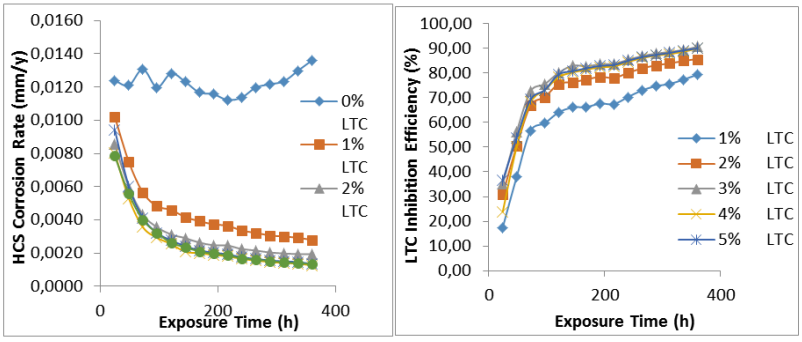

(a) (b)

Figure 8. Plot of (a) HCS corrosion rate versus exposure time in 1 M H_2SO_4 (b) LTC inhibition efficiency versus exposure time in 1 M H_2SO_4.

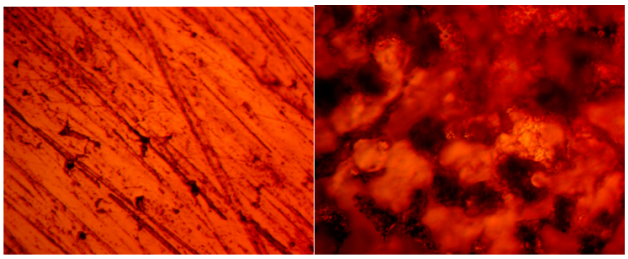

(a) (b)

Figure 9. Micro-analytical images of HCS at mag. x100 (a) before corrosion, (b) after corrosion in 0% LTC/1 M H_2SO_4 solution.

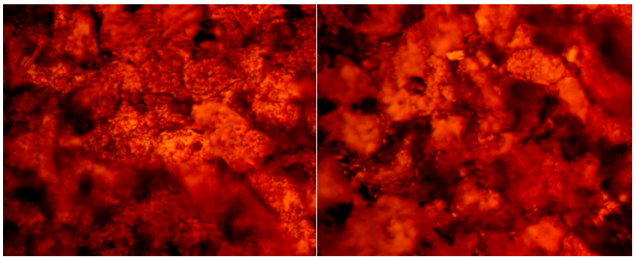

(a) (b)

Figure 10. Micro-analytical images of HCS at mag. x100 (a) after corrosion in 1% LTC/1 M H_2SO_4, (b) after corrosion in 5% LTC/1 M H_2SO_4.

Statistical studies

The statistical result in Table 5 showed that both LTC concentration and exposure time are statistically relevant variables responsible for HCS corrosion rate values with calculated *F*-values (mean square ratio) of 51.79 and 437.28. These values are significantly greater than the theoretical significance factor (significance *F*) value of 3.01, corresponding to a percentage significance of 10.50% and 88.69%. However, the results of the percentage significance factor also show that exposure time is the dominant factor responsible for the electrochemical behavior and the resulting microstructural properties of HCS with respect to changes in LTC concentration. Changes in LTC concentration have limited influence on its corrosion inhibition performance as it tends to be effective at all concentrations studied. The performance of the inhibitor tends to be time-dependent rather than concentration-dependent, especially within the first 120 h.

Table 5. Analysis of variance for HCS in 1 M H_2SO_4/ (1%-5% LTC) at 95% confidence level.

Source of Variation	Sum of Squares	Degree of Freedom	Mean Square	Mean Square Ratio (F)	Significance F	F (%)
LTC Concentration	863.40	4	215.85	51.79	3.01	10.50
Exposure Time	7289.90	4	1822.48	437.28	3.01	88.69
Residual	66.68	16	4.17			
Total	8219.99	24				

Conclusion

The study of the synergistic effect of L-leucine and trypsin complex on the corrosion inhibition of high carbon steel in H_2SO_4 solution showed the admixture to be highly effective at all range of concentrations studied from potentiodynamic polarization analysis and weight loss measurement. Corrosion inhibition efficiency was time-dependent as the results were not proportional to inhibitor concentration. Chemisorption adsorption mechanism occurred on the steel surface according to isotherms determined with near unity correlation coefficient. Identified functional groups were completely adsorbed onto both steels from analysis of the adsorption spectra. Optical images of the inhibited steel showed mild deterioration with fewer and very shallow pits compared to the uninhibited counterparts with severely corroded morphology.

Acknowledgement

The author acknowledges Covenant University Ota, Ogun State, Nigeria for the sponsorship and provision of research facilities for this project.

References

1. Singh, D.K.; Kumar, S.; Udayabhanu, G.; John, R.P. 4(N,N-dimethylamino) benzaldehyde nicotinic hydrazone as corrosion inhibitor for mild steel in 1M HCl solution: An experimental and theoretical study. *J. Mol. Liqs*. **2016**, *216*, 738–746. DOI: https://doi.org/10.1016/j.molliq.2016.02.012.

2. Alaneme, K.K.; Olusegun, S.J.; Adelowo, O.T. Corrosion inhibition and adsorption mechanism studies of Hunteria umbellata seed husk extracts on mild steel immersed in acidic solutions. *Alexandria Eng. J*. **2016**, *55* (1), 673–681. DOI: https://doi.org/10.1016/j.aej.2015.10.009.

3. Fiori-Bimbi, M.V.; Alvarez, P.E.; Vaca, H.; Gervasi, C.A. Corrosion inhibition of mild steel in HCl solution by pectin. *Corros. Sci*. **2015**, *92*, 192–199. DOI: https://doi.org/10.1016/j.corsci.2014.12.002

4. Roberge, P.R. Handbook of corrosion engineering, McGraw-Hill, New York, 2000.

5. Ansari, K.R.; Quraishi, M.A.; Singh, A. Chromennopyridin derivatives as environmentally benign corrosion inhibitors for N80 steel in 15% HCl. *J. Ass. Arab Univ. Basic & App. Sci*. **2015**, *22*, 45-54. DOI: https://doi.org/10.1016/j.jaubas.2015.11.003.

6. Samuel, M.; Sengul, M. Stimulate the Flow. *Middle East & Asia Reserv. Rev.* **2003**, *3*, 40–53.

7. Kamal, C.; Sethuraman, M.G. *Spirulina platensis* - A novel green inhibitor for acid corrosion of mild steel. *Arabian J. Chem*. **2012**, *5* (2), 155-161. DOI: https://doi.org/10.1016/j.arabjc.2010.08.006.

8. Okafor, P.C.; Ikpi, M.E.; Uwah, I.E.; Ebenso, E.E.; Ekpe, U.J.; Umoren, S.A. Inhibitory action of *Phyllanthus amarus* extracts on the corrosion of mild steel in acidic media. *Corros. Sci*. **2008**, *50* (8), 2310-2317. DOI: https://doi.org/10.1016/j.corsci.2008.05.009.

9. Singh, A.; Singh, V.K.; Quraishi, M.A. Effect of fruit extracts of some environmentally benign green corrosion inhibitors on corrosion of mild steel in hydrochloric acid solution. *J. Mats. & Environ. Sci*. **2010**, *1* (3), 162-174.

10. Singh, A.; Ebenso, E.E.; Quraishi, M.A. Corrosion inhibition of carbon steel in HCl solution by some plant extracts. *Int. J. Corrosion*. **2012**, 897430. DOI: https://doi.org/10.1155/2012/897430.

11. Loto, R. T. Corrosion inhibition studies of the combined admixture of 1, 3-diphenyl-2-thiourea and 4-hydroxy-3-methoxybenzaldehyde on mild steel in dilute acid media. *Rev. Colomb. Quim*. **2017**, *46* (1), 20-32. DOI: https://doi.org/10.15446/rev.colomb.quim.v46n1.59578.

12. Raja, P.B.; Sethuraman, M.G. Natural products as corrosion inhibitor for metals in corrosive media - A review. *Mats. Letts*. **2008**, *62* (1), 113-116. DOI: https://doi.org/10.1016/j.matlet.2007.04.079.

13. Loto, C.A.; Loto, R.T.; Popoola, A.P.I. Synergistic effect of tobacco and kola tree extracts on the corrosion inhibition of mild steel in acid chloride. *Int. J. Electrochem. Sci.* **2011**, *6*, 3830 – 3843.

14. Loto, C.A.; Loto, R.T.; Joseph, O.O.; Popoola, A.P.I. Corrosion Inhibitive Behaviour of Camellia Sinensis on Aluminium Alloy in H_2SO_4. *Int. J. Electrochem. Sci*. **2014**, *9*, 1221 – 1231.

15. ASTM G1 – 03. Standard practice for preparing, cleaning, and evaluating corrosion test specimens. 2011. Retrieved May 5, 2017, from http://www.astm.org/Standards/G1.

16. ASTM G102 - 89. Standard practice for calculation of corrosion rates and related information from electrochemical measurements. 2015. Retrieved May 5, 2017, from http://www.astm.org/Standards/G31.

17. Choi, Y.; Nesic, S.; Ling, S. Effect of H2S on the CO2 corrosion of carbon steel in acidic solutions. *Electrochim. Acta*. **2011**, *56* (4), 1752-1760. DOI: https://doi.org/10.1016/j.electacta.2010.08.049.

18. ASTM G31 – 12a. Standard practice for laboratory immersion corrosion testing of metals. 2012. Retrieved May 5, 2017, from https://www.astm.org/DATABASE.CART/HISTORICAL/G31-72R04.htm.

19. Venkatesan, P.; Anand, B.; Matheswaran, P. Influence of formazan derivatives on corrosion inhibition of mild steel in hydrochloric acid medium. *E-Journal of Chemistry*, **2009**, *6* (S1), S438-S444. DOI: https://doi.org/10.1155/2009/507383.

20. Schutt, H.U.; Horvath, R.J. *Crude column overhead corrosion problem caused by oxidized sulfur species*. NACE, Houston, Texas, 1987.

21. Schofield, M.J. *Plant Engineer#s Reference Book*, Elsevier, 2003.

22. Cao, C. On electrochemical techniques for interface inhibitor research, Corros. Sci. 1996, 38 2073-2082. DOI: https://doi.org/10.1016/s0010-938x(96)00034-0.

23. Loto, R.T. Corrosion inhibition performance of the synergistic effect of rosmarinus officinalis and 5-bromovanillin on 1018 carbon steel in dilute acid media. *J. Fail. Anal. & Preven*. **2017**, *17* (5), 1031-1043. DOI: https://doi.org/10.1007/s11668-017-0334-z.

24. Loto, R.T.; Loto, C.A.; Popoola. A.P.I. Inhibition effect of deanol on mild steel corrosion in dilute sulphuric acid. *South African J. Chem*. **2015**, *68*, 105-114. DOI: https://doi.org/10.17159/0379-4350/2015/v68a16.

25. Limousin, G.; Gaudet, J.P.; Charlet, L.; Szenknect, S.; Barthes, V.; Krimissa M. Sorption isotherms: A review on physical bases, modeling and measurement. *Appl. Geochem*. **2007**, *22* (2), 249–275. DOI: https://doi.org/10.1016/j.apgeochem.2006.09.010.

26. Allen, S.J.; Mckay, G.; Porter, J.F. Adsorption isotherm models for basic dye adsorption by peat in single and binary component systems. *J. Colloid & Inter. Sci*. **2004**, *280* (2), 322–333. DOI: https://doi.org/10.1016/j.jcis.2004.08.078.

27. Guidelli, R. *Adsorption of molecules at metal electrodes*, Kowski, J.L.; Ross. P.N. VCH Publishers lnc., New York, 1, 1992.

28. Hosseini, M.; Stijn, F.L.M.; Mohammed, R.A. Synergism and antagonism in mild steel corrosion inhibition by sodium dodecylbenzenesulphonate and hexamethylenetetramine. *Corros. Sci*. **2003**, *45* (7), 1473–1489. DOI: https://doi.org/10.1016/s0010-938x(02)00246-9

29. Ashish, K.S.; Quraishi, M.A. Investigation of the effect of disulfiram on corrosion of mild steel in hydrochloric acid solution. *Corros. Sci*. **2011**, *53*(4), 1288-1297. DOI: https://doi.org/10.1016/j.corsci.2011.01.002.

30. Zeldowitsch, J. Adsorption site energy distribution. *Acta Physicochim. URSS.* **1934**, *1*, 961–973.

31. Aharoni, C.; Ungarish, M. Kinetics of activated chemisorption. Part 2. Theoretical models, *J. of Chem. Soc. Faraday Trans. 1: Phys. Chem. in Condensed Phases*. **1977**, 73, 456–464. DOI: https://doi.org/10.1039/f19777300456.

32. Loto, R.T. Corrosion inhibition of mild steel in acidic medium by butyl alcohol, *Res. on Chem. Interm*. **2014**, *40*(5), 1899–1910. DOI: https://doi.org/10.1007/s11164-013-1088-1.

33. Loto, R.T.; Loto, C.A.; Fedotova, T. Electrochemical studies of mild steel corrosion inhibition in sulfuric acid chloride by aniline. *Res. Chem. Interm*. **2014**, *40*(4), 1501–1516. DOI: https://doi.org/10.1007/s11164-013-1055-x.

34. Table of Characteristic IR Absorptions. Retrieved January 12, 2017, from http://orgchem.colorado.edu/Spectroscopy/specttutor/irchart.pdf.

35. George, S. *Infrared and Raman Characteristic Group Frequencies: Tables and Charts*. John Wiley & Sons, New York, **2004**.

Alternative link

https://revistas.unal.edu.co/index.php/rcolquim/article/view/68058 (html)